ANALYTICAL THEORY FOR EXTRACELLULAR ELECTRICAL STIMULATION OF NERVE WITH FOCAL ELECTRODES

I. Passive Unmyelinated Axon

J. T. RUBINSTEIN AND F. A. SPELMAN
Regional Primate Research Center, University of Washington, Seattle, Washington 98195; and
Eaton-Peabody Laboratory, Massachusetts Eye and Ear Infirmary, Boston, Massachusetts 02114

ABSTRACT The cable model of a passive, unmyelinated fiber in an applied extracellular field is derived. The solution is valid for an arbitrary, time-varying, applied field, which may be determined analytically or numerically. Simple analytical computations are presented. They explain a variety of known phenomena and predict some previously undescribed properties of extracellular electrical stimulation. The polarization of a fiber in an applied field behaves like the output of a spatial high-pass and temporal low-pass filter of the stimulus. High-frequency stimulation results in a more spatially restricted region of fiber excitation, effectively reducing current spread relative to that produced by low-frequency stimulation. Chronaxie measured extracellularly is a function of electrode position relative to the stimulated fiber, and its value may differ substantially from that obtained intracellularly. Frequency dependence of psychophysical threshold obtained by electrical stimulation of the macaque cochlea closely follows the frequency dependence of single-fiber passive response.

1. INTRODUCTION

There is an extensive body of mathematical theory describing the passive and active electrical properties of neurons (8, 21). The vast majority of the theory available considers only intracellular stimulation, as this mode is of greatest concern to the classical biophysicist. Rushton (16, 17) and others (4) gave early consideration to the problem of extracellular stimulation. More recently, a number of authors have attempted to define the passive response of nerve and muscle to applied fields (1, 2, 10, 13, 14, 20, 22).

With the exception of McNeal's model (10), and the theoretical development of Tranchina and Nicholson (22), all prior work in this area restricted either the location of the source electrodes or their time-dependent behavior. Tranchina and Nicholson have developed an elaborate theory describing the polarization of entire neurons by arbitrary applied fields but their calculations are restricted to spatially uniform stimuli. McNeal's contribution was the first model valid for an arbitrary, time-varying, externally applied field. Without detracting from the importance of its results, this model has two significant weaknesses: (*a*) Internodal impedance is ignored, and the "effect of current leaking through the myelin sheath . . . is difficult to assess without resorting to a much more complex simulation. . ." (*b*) Whereas the results of the numerical simulations are most informative, the numerical solution itself yields little insight into the phenomenon of extracellular stimulation.

As electrical stimulation of myelinated fibers is a frequent experimental procedure in mammalian neurophysiology and is also of great clinical importance, mathematical modeling of extracellular stimulation of unmyelinated fibers has essentially been ignored. This omission is unfortunate because the problem is analytically tractable to some degree and provides much insight into the general problem of extracellular electrical stimulation of nerve. The goal of this study is to present a "systems" approach to the problem. A model of the passive fiber constitutes the "system" to which the arbitrary time-varying field may be applied as an input function. The output "signal" is the membrane polarization induced by the response of the "system" to the applied field.

Because the passive behavior of each node in a myelinated fiber should be comparable with that of a segment of unmyelinated axon of equal diameter, the concepts derived here should also apply to myelinated fibers in a qualitative manner. The development of a myelinated fiber

Address correspondence to Jay T. Rubinstein, M.D., Ph.D., Dept. of Surgery, Beth Israel Hospital, 330 Brookline Avenue, Boston, MA 02215.

model using these techniques has been completed and will be reported in a future publication.

2. THEORY

2.1 Arbitrary External Field

Fig. 1 shows a passive cable model of an unmyelinated fiber with intracellular potential $V(x, t)$ in an applied field $\Psi(x, t)$. $V(x, t)$ is defined as the excursion of the intracellular potential from the resting value so that at rest, $V(x, t) = 0$. This is similar to Hermann's cable model of an axon (19), but includes the applied extracellular field. Developed on the basis of McNeal's approach (10), it results in a partial differential equation describing the entire fiber rather than a set of ordinary differential equations, each describing a single node/internode unit.

Choosing a fiber of radius a and defining the membrane potential as $V_m(x, t) = V(x, t) - \Psi(x, t)$, it is straightforward to show the following relations.

$$i_m = c_m \frac{\partial V_m}{\partial t} + \frac{V_m}{r_m}$$

$$\frac{\partial i_a}{\partial_x} = -i_m$$

$$\frac{\partial V}{\partial_x} = -i_a r_a,$$

where i_m is the membrane current in A/cm, i_a is the axial current in amperes, $r_m = R_m/2\pi a$, $c_m = 2\pi a\, C_m$, and $r_a = R_a/\pi a^2$. These are manipulated to yield the partial differential equation describing the intracellular potential

$$-\lambda^2 V_{xx} + \tau V_t + V = \tau \Psi_t + \Psi, \tag{1}$$

where the space constant $\lambda = \sqrt{r_m/r_a}$ and the time constant $\tau = r_m c_m$. Eq. 1 is the inhomogeneous, one-dimensional, heat or diffusion equation. The inhomogeneous term is a function of the applied field.

Solving the above equation requires the establishment of boundary conditions, initial conditions, and the choice of a forcing function. Specifying a closed axon greatly simplifies the solution so the axial current is set to zero at $x = 0$.

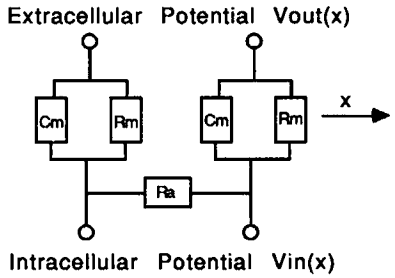

FIGURE 1 The modified cable model. In the text, $V = V_{in}$ and $\Psi = V_{out}$. R_m is the specific membrane resistance in Ω cm^2. C_m is the specific membrane capacitance in μF/cm^2. R_a is the resistivity of the cytoplasm in Ω cm. x is distance along the fiber in centimeters.

This constrains the present analysis to problems possessing axial symmetry about $x = 0$. Let the membrane potential be zero at $t = 0$, and let us assume the external medium is purely resistive so that a quasistatic approximation applies, or $\Psi(x, t) = u(x)w(t)$. Taking both the cosine transform in x and Laplace transform in t(3) of Eq. 1 and examining the time impulse response $w(t) = \delta(t)$ yields

$$(1 + s\tau + k^2\lambda^2)\bar{\bar{V}}(k,s) = \bar{u}(k)(1 + s\tau)$$

or

$$\bar{\bar{V}}(k,s) = \bar{u}(k)\,\frac{1 + s\tau}{1 + k^2\lambda^2 + s\tau},$$

where $\bar{\bar{V}}$ is the Laplace transform in t and cosine transform in x of $V(x, t)$; $\bar{u}$ is the cosine transform in x of $u(x)$. Noting that

$$\bar{\bar{V}}_m = \bar{\bar{V}} - \bar{\bar{\Psi}}$$

and inverting the Laplace transform (3) yields the impulse response

$$\bar{V}_m(k, t) = \bar{u}(k)\,\frac{-k^2\lambda^2}{\tau}\,e^{-(1+k^2\lambda^2)t/\tau}. \tag{2}$$

If instead of inverting the transform, allowing $s = j\omega$ gives the Fourier spatial and time frequency representation of the system response

$$\bar{\bar{V}}_m(k, \omega) = H(k, \omega)\bar{u}(k), \tag{3}$$

where

$$H(k, \omega) = \frac{(-k^2\lambda^2)\,(1 + k^2\lambda^2 - j\omega\tau)}{(1 + k^2\lambda^2)^2 + \omega^2\tau^2}. \tag{4}$$

Computing the magnitude and phase of Eq. 4 gives the spatial and time frequency response magnitude and phase of the fiber model

$$|H(k, \omega)| = \frac{k^2\lambda^2}{\sqrt{(1 + k^2\lambda^2)^2 + \omega^2\tau^2}} \tag{5}$$

$$\Phi[H(k, \omega)] = \arctan\left(-\frac{\omega\tau}{1 + k^2\lambda^2}\right). \tag{6}$$

The step response of the system, $S_m(x, t)$, is easily obtained by integration with respect to time of the impulse response given by Eq. 2.

$$\bar{S}_m(k, t) = \bar{u}(k)\,\frac{-k^2\lambda^2}{1 + k^2\lambda^2}\,(1 - e^{-(1+k^2\lambda^2)t/\tau}). \tag{7}$$

2.2 Simulation

Eqs. 2–4 allow the computation of the response to an arbitrary stimulus using the usual time or frequency domain operations. The cosine transform in x, $\bar{u}(k)$, of the applied field $u(x)$, must be obtained first. A simple analytical example is given by letting $\bar{u}(k) = -1$. The

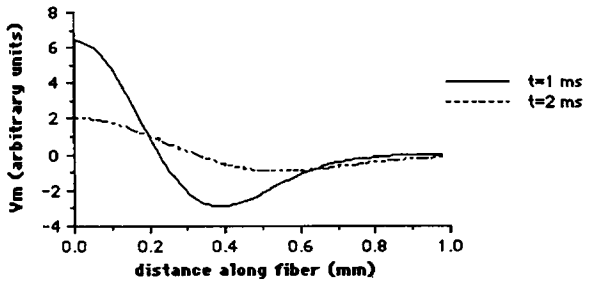

FIGURE 2 Simulated spatial and temporal impulse response of a 1-μm-diameter fiber at the two times specified in the plot. V_m is the induced membrane polarization as given by Eq. 8.

inverse cosine transform of Eq. 2, given by (3.952) in reference 6 and some manipulation yields

$$V_m(x,t) = \frac{2\lambda^2 \frac{t}{\tau} - x^2}{4\sqrt{\pi}\tau\lambda^3 (t/\tau)^{5/2}} \exp\left(-t/\tau - \frac{x^2\tau}{4\lambda^2 t}\right). \quad (8)$$

This is the spatial and time impulse response of the fiber. It corresponds to the time impulse response of a fiber to an infinitely negative applied field at $x = 0$ and a zero applied field everywhere else. It could be convolved numerically in both space and time with the applied field, $\Psi(x,t)$, to determine the fiber response to an arbitrary stimulus. Alternatively a plot of Eq. 8 will reveal some general properties of the solution. An axon diameter of 1 μm is chosen to be comparable with a macaque auditory nerve fiber. These fibers were studied by Gacek and Rasmussen (5), who demonstrated a unimodal distribution of 1–8 μm, with a mode of 3 μm. Because the ratio of axon to fiber diameter must be ~0.6 (8), the axon distribution ranges from 0.6 to 4.8 μm, with a mode of 1.8 μm. R_m and C_m are chosen to be 10 $K\,\Omega cm^2$ and 1 $\mu F/cm^2$, respectively (8).

3. RESULTS: VERIFICATION OF KNOWN PROPERTIES

3.1 Anodal Block and Site of Stimulation

Fig. 2 demonstrates that for a negative applied field, the fiber is depolarized near the source and hyperpolarized at some distance from the source. This phenomenon is responsible for the "anodal block" described by Ranck (14), in which a suprathreshold cathodal stimulus may cause conduction block. A necessary corollary is that anodal stimuli have higher thresholds than cathodal stimuli, and threshold is reached at a different site. Thus bipolar or biphasic stimuli can cause threshold to be reached at more than one site along a fiber. Measurements of conduction velocity should take this into account.

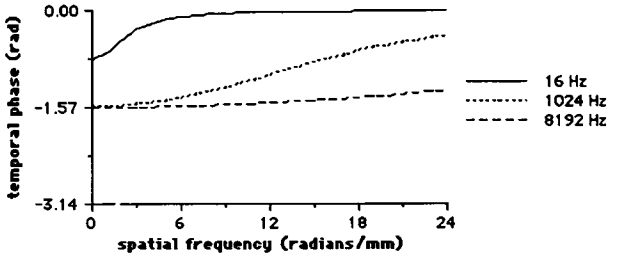

FIGURE 4 Spatial frequency phase response of fiber model at the three temporal frequencies indicated in the plot.

3.2 Spatial/Temporal Interdependence

Plots of the magnitude and phase response of $H(k, \omega)$, Eqs. 5 and 6, are given in Figs. 3 and 4, respectively. The polarization of the fiber behaves like a spatial high-pass and temporal low-pass filter of the applied field. Four important features of this filter should be noted: (*a*) Fibers respond most vigorously to stimuli with low temporal frequencies and high spatial frequencies. (*b*) Stimuli rich in high spatial frequencies will be more resistant to the decreased fiber response caused by increases in temporal frequency than will stimuli with less high spatial frequency content. (*c*) Phase delay is increased with increasing temporal frequency or decreasing spatial frequency. (*d*) Stimuli rich in high spatial frequencies will be more resistant to the increased phase delay caused by increases in temporal frequency than will stimuli with less high spatial frequency content.

3.3 Longitudinal and Transverse Current

The four principles above explain much that is known about extracellular stimulation and some phenomena not yet reported. To fully appreciate their significance a specific problem must be examined, placing bipolar pairs of point current sources near the fiber as illustrated in Fig. 5. Because passive, subthreshold behavior is the concern, it

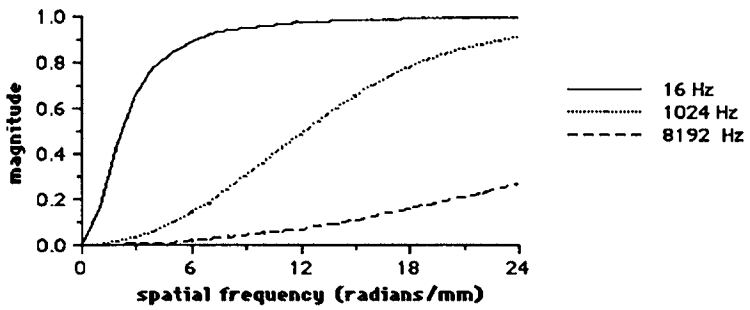

FIGURE 3 Spatial frequency magnitude response of fiber model $|H(k,\omega)|$, at the three temporal frequencies indicated in the plot. Increasing temporal frequency increases the cutoff frequency of this spatial high-pass filter.

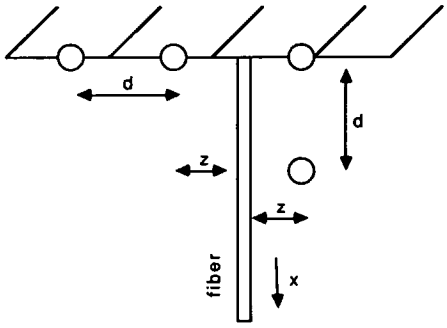

FIGURE 5 A semiinfinite fiber near perpendicular and parallel bipolar current sources. Electrode separation is d. Distance from the closest source to the fiber is z.

may be assumed that the fiber does not alter the external field, determined strictly from the bipolar source. The source and fiber are placed in the same plane and because we will be computing relative results, the injected current and resistivity of the medium need not be specified. Fig. 6 illustrates the extracellular potential along the fiber for dipoles oriented perpendicular and parallel to it.

Referring back to Fig. 5, note the symmetry in x in these rectangular coordinates. The spatial frequency content of a point source is given by the cosine transform and equation (3.754) in reference 6,

$$\int_0^\infty \frac{\cos kx}{\sqrt{x^2 + z^2}}\, dx = K_0(k|z|),$$

where K_0 is the modified Bessel function of the second kind, order zero. Thus the spatial frequency content of a dipole oriented perpendicular to the fiber is given by

$$\bar{u}(k) = K_0(k|z|) - K_0(k|z + d|) \tag{9}$$

and for a dipole parallel to the fiber by

$$\bar{u}(k) = K_0(k|z|)\,(1 - \cos kd). \tag{10}$$

Plots of Eqs. 9 and 10, given in Fig. 7, explain one of Rushton's (16) experimental findings. A fiber-oriented parallel to a dipole has a lower threshold than one perpendicular to it because the parallel dipole is richer in high spatial frequencies. This is somewhat comparable with saying that the parallel dipole generates a greater voltage

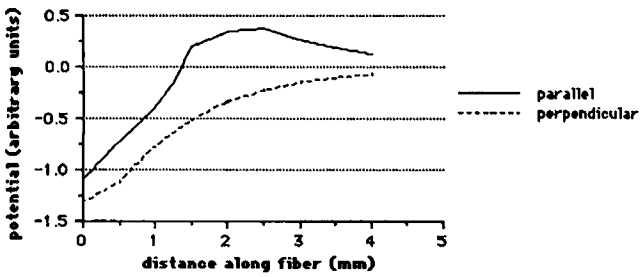

FIGURE 6 Extracellular potential along fiber for perpendicular and parallel bipolar current sources. d = 2 mm, z = 1 mm.

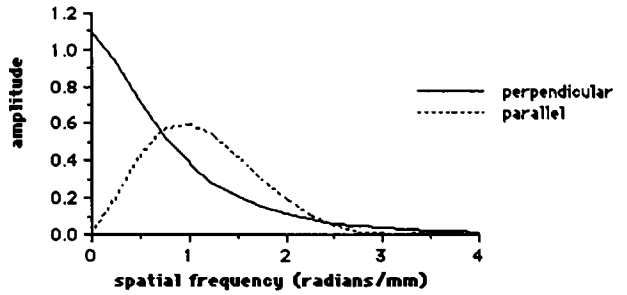

FIGURE 7 Spatial frequency content of perpendicular and parallel dipoles. d = 2 mm, z = 1 mm. The parallel dipole has greater energy in the high spatial frequencies.

gradient or current density in the direction of the fiber. The crucial distinction is that spatial frequency content is much easier to calculate for any given geometry than is current density. The effect is demonstrated more clearly by multiplying Eqs. 9 and 10 by Eq. 4, as shown in Fig. 8. Thus the spatial frequency content of the applied potential field is the most important parameter in determining its "excitatory capacity," or its ability to polarize a fiber in its vicinity.

3.4 The Strength-Length Curve

Another of Rushton's findings was the "strength-length" curve, which demonstrated that fiber threshold decreased as the dipole separation increased, up to a point, then remained constant. This effect is explained by Fig. 9, which shows the spatial frequency content of a parallel dipole as the separation increases. Note that the overall amplitude increases continuously as the separation increases, but the location of the peak spatial frequency component decreases. Because of the high-pass nature of the membrane, the fiber response will saturate at some degee of separation. A similar effect occurs with a perpendicular dipole.

3.5 Fiber Distance and Current Spread

Cochlear implant researchers long have known that electrodes close to their target neurons have greater spatial specificity, or less "current spread," than more distant

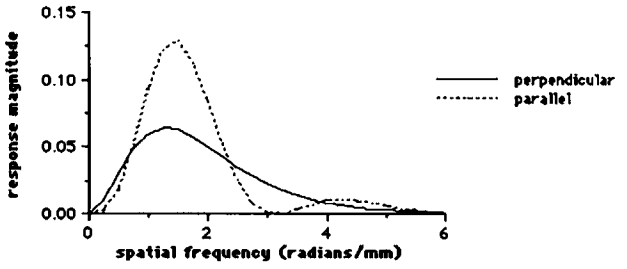

FIGURE 8 Spatial frequency representation of fiber response, $|H(k, \omega)\bar{u}(k)|$, to perpendicular and parallel dipoles at a temporal frequency of 16 Hz. d = 2 mm, z = 1 mm. The system response is more vigorous to a parallel dipole.

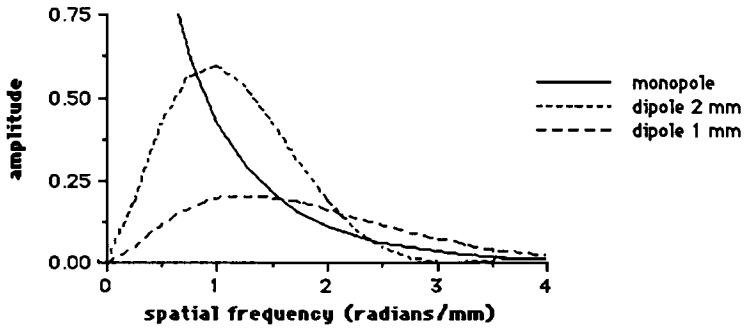

FIGURE 9 Effect of parallel dipole separation on spatial frequency content of stimulus. $z = 1$ mm. Separation of 1 mm, 2 mm, and ∞, a monopole. Note that the monopole has an infinite DC spatial frequency component.

electrodes (23). Fig. 10 illustrates the effect of increasing the distance of a monopole from a fiber. The more distant stimulus has lower amplitude at all spatial frequencies, but it suffers a relatively greater decrement in its high spatial frequencies. From simple considerations of the relation between the space and spatial frequency domains, it is clear that a stimulus rich in high spatial frequency content, or broadband in the spatial frequency domain, must have less "current spread," or be narrowband in the space domain. Thus, considerations of spatial frequency content are extremely useful in describing current spread.

4. RESULTS: PREDICTED PHENOMENA

4.1 Stimulus Frequency and Current Spread

The above discussion of the effect of stimulus distance on spatial frequency content implies a phenomenon that has not yet been reported. Fig. 3 illustrates that fibers responding to stimuli rich in high spatial frequencies will be less sensitive to increased temporal frequency. Thus increasing the temporal frequency of a stimulus will increase the threshold of distant fibers more than the threshold of near fibers. In other words, high-frequency stimuli result in less effective current spread than low-frequency stimuli even with a purely resistive external medium. Fig. 11 shows that fibers near the source exhibit shorter time constants than do distant fibers. The impulse response of a distant fiber decays with the same time constant as a space-clamped fiber, i.e., the specific membrane time constant $\tau = r_m c_m$.

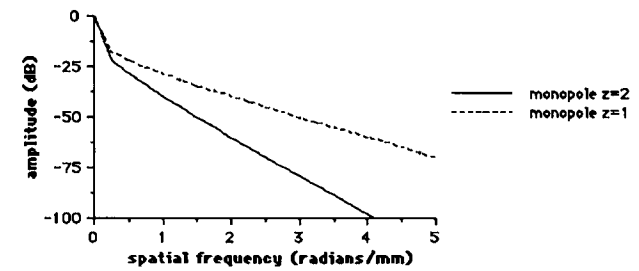

FIGURE 10 Effect of distance of a monopolar source on its spatial frequency content. The more distant source has less high spatial frequency content.

4.2 Stimulus Distance and Response Phase

Similar arguments as given in Section 4.1 imply that more distant fibers will respond with greater phase lag than will closer fibers. This effect becomes more prominent as stimulus frequency is increased and is independent of the increase in threshold with distance. It suggests that fiber synchrony depends on the spatial distribution of the fibers stimulated and the frequency of stimulation.

4.3 Stimulus Frequency and Psychophysical Threshold of Cochlear Implants

The question arises as to whether our simple model describing the passive electrical properties of a single fiber can accurately reproduce the psychophysical response of the electrically stimulated cochlea. The relation between psychophysical threshold, the current required to evoke trained behavior in an alert animal, and stimulus frequency has been reported for the macaque (12). If it is assumed that all spiral ganglion fibers have similar active properties, that is, similar voltage-dependent channel densities, kinetics, and ionic gradients,[1] then their membrane threshold, defined as the membrane depolarization at which an action potential occurs, should also be similar. Under these conditions, the relative threshold between two stimulation paradigms will be determined by the relative peak passive responses induced in the membrane potential by the stimulation. We may thus attempt to model the relation between single fiber threshold and frequency by examining the relative peak response as a function of frequency (this assumes that accommodation is not significant).

To avoid the use of numerical methods, rather than computing the peak fiber response as a function of frequency, we will determine the dominant spatial frequency component and study its behavior as a function of frequency. Fig. 8 demonstrates that for the perpendicular dipole

[1]This assumption is probably incorrect because it has been shown that action currents in small myelinated axons are not as intense as in larger myelinated axons (11). The necessary voltage-clamp studies have not been performed in auditory nerve fibers so there is no way to evaluate the validity of this assumption.

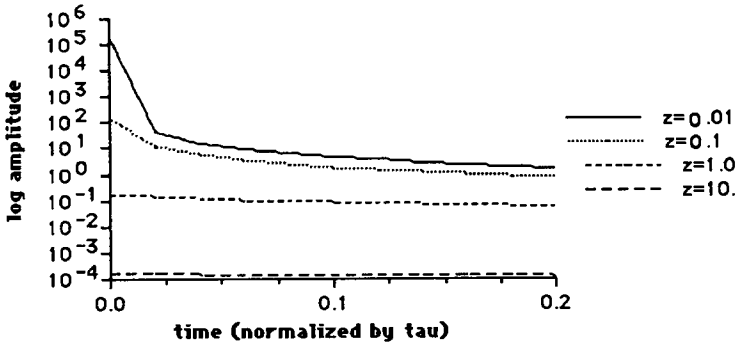

FIGURE 11 Impulse response (depolarization) of an infinitely long fiber at the position nearest a monopolar, cathodal point source for four different cathodal distances. Time is normalized to τ, the specific membrane time constant, and distance normalized to λ, the length constant. Distant fibers' impulse responses decay with time constant τ; near fibers have shorter time constants.

geometry of Fig. 5, not an unreasonable approximation to the stimulation scheme employed by Pfingst (12), $k = 1.5$ is the dominant spatial frequency component of the fiber response. This holds throughout the range of frequencies employed in Fig. 2 of reference 12. The relative decrease in the system response to $k = 1.5$ is plotted in Fig. 12 alongside the relative increase in psychophysical threshold, both as a function of frequency.

4.4 Strength-Duration Curves

Because we have ignored active membrane properties, a true strength-duration curve cannot be computed as we have no way of calculating the rheobase current. However, if we normalize passive fiber response to a putative rheobase current, we may calculate a relative strength-duration curve from which a chronaxie may be determined. This curve is the reciprocal of the step response given in Eq. 7 if similar assumptions are made as in Section 4.3. Rather than actually compute the fiber response, we could determine the dominant spatial frequency component for the durations of interest and plot its strength-duration curve. Our purposes are better served by simply plotting the strength-duration curve for several spatial frequencies in Fig. 13.

Examination of Fig. 13 demonstrates another fundamental difference between intracellular and extracellular stimulation. With extracellular stimulation, chronaxie is strongly dependent on the spatial frequency content, or geometry of the stimulation apparatus. It has been shown that the intracellular step response of a cable stimulated at a point demonstrates a shorter time constant than a uniformly polarized cable, reaching 84% of its steady-state value at $t = \tau$ (8). Using Eq. 7 and a 1-μm-diameter fiber, an extracellular stimulation paradigm where the dominant spatial frequency is $k = 1.8$ will lead to approximate agreement between intracellular and extracellular measurements of chronaxie. If the dominant spatial frequency component is higher than $k = 1.8$, the extracellular chronaxie will be less than the intracellular chronaxie. This may well explain the discrepancy noted by Ranck in his review (14).

5. DISCUSSION

We have developed an analytical model for extracellular stimulation of passive, unmyelinated axon. The theory explains many of the known properties of extracellular stimulation and suggests behavior that has not yet been described. The predictions are: (*a*) Increasing stimulus frequency improves the spatial selectivity of the stimulus. (*b*) Distant fibers will have greater phase lag than near fibers. (*c*) Strength-duration curves for extracellular stimulation may be different from the same curves measured intracellularly and are a function of electrode placement. (*d*) The increase in psychophysical threshold with frequency of electrical stimulation of the auditory nerve of the macaque follows the decreased passive response of a single fiber.

These phenomena could be exploited in both clinical and basic applications of extracellular stimulation if they can be verified experimentally. Prediction 1 may have substantial impact on all forms of functional electrical stimulation

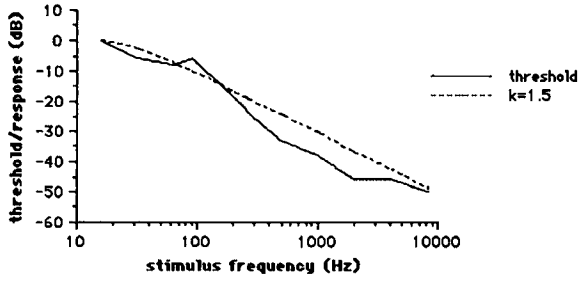

FIGURE 12 Psychophysical threshold increase relative to threshold at 16 Hz and response decrease of $k = 1.5$ relative to response of $k = 1.5$ at 16 Hz, both as a function of stimulus frequency.

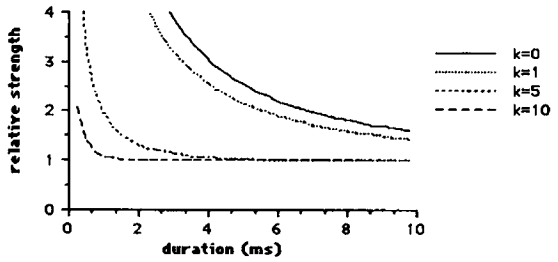

FIGURE 13 Relative strength-duration curves for a variety of spatial frequencies. Curves are plotted so the rheobase is 1.

where the minimization of current spread is desirable (7). Further modeling for the specific application and experimental verifications are necessary for this prediction to be useful. Prediction 2 suggests that for low-frequency stimulation of the auditory nerve, fiber synchronization (9, 18) may be a function of fiber distance. This prediction also suggests that phased-array approaches to functional electrical stimulation may prove useful as a means of "focusing" currents. Prediction 3 explains the discrepancies that have been noted between intracellular and extracellular chronaxies (14). It reemphasizes the importance of determining the conduction velocity and reporting the geometry of the stimulation apparatus when extracellular strength-duration curves are measured.

The model is flexible in that it is easily merged with either analytical or numerical solutions for the applied field and the inverse cosine transform is obtained simply by a fast Fourier transform. These numerical calculations have been performed for a variety of finite-sized stimulation electrodes and the results will be reported elsewhere. The techniques required to develop an integrated electrode/volume conduction/neural model for electrical stimulation of the cochlea have been described (15).

Wade Smith read an early version of the manuscript.

This work was supported by National Institutes of Health grants GM07266, RR00166, and NS13056, a subcontract to the University of Washington from the University of Michigan.

Received for publication 1 February 1988 and in final form 22 June 1988.

REFERENCES

1. Abzug, C., M. Maeda, B. W. Peterson, and V. J. Wilson. 1974. Cervical branching of lumbar vestibulospinal axons. *J. Physiol. (Lond.)*. 243:499–522.
2. Bement, S. L., and J. B. Ranck, Jr. 1969. A model for electrical stimulation of central myelinated fibers with monopolar electrodes. *Exp. Neurol.* 24:171–186.
3. Churchill, R. V. 1972. Operational Mathematics. 3rd ed. McGraw-Hill Book Co., New York.
4. Cole, K. S., and R. F. Baker. 1941. Longitudinal impedance of squid giant axon. *J. Gen. Physiol.* 24:771–788.
5. Gacek, R. R., and G. L. Rasmussen. 1961. Fiber analysis of the statoacoustic nerve of guinea pig, cat, and monkey. *Anat. Rec.* 139:455–463.
6. Gradshteyn, I. S., and I. M. Ryzhik. 1980. Table of Integrals, Series, and Products. Academic Press, Orlando, FL.
7. Hambrecht, F. T. 1979. Neural prostheses. *Annu. Rev. Biophys. Bioeng.* 8:239–267.
8. Jack, J. J. B., D. Noble, and R. W. Tsien. 1983. Electric Current Flow in Excitable Cells. Clarendon, Oxford.
9. Kiang, N. Y. S., and E. C. Moxon. 1972. Physiological considerations in artificial stimulation of the inner ear. *Ann. Otol. Rhinol. & Laryngol.* 81:714–730.
10. McNeal, D. R. 1976. Analysis of a model for excitation of myelinated nerve. *IEEE Trans. Biomed. Eng.* BME-23:329–337.
11. Paintal, A. S. 1966. The influence of diameter of medullated nerve fibers of cats on the rising and falling phases of the spike and its recovery. *J. Physiol. (Lond.)*. 184:791–811.
12. Pfingst, B. E., I. Glass, F. A. Spelman, and D. Sutton. 1985. Psychophysical studies of cochlear implants in monkeys: clinical implications. *In* Cochlear Implants. R. A. Schindler and M. M. Merzenich, editors. Raven Press, New York. 305–321.
13. Ranck, J. B., Jr. 1963. Analysis of specific impedance of rabbit cerebral cortex. *Exp. Neurol.* 7:153–174.
14. Ranck, J. B., Jr. 1975. Which elements are excited in electrical stimulation of mammalian central nervous system: a review. *Brain Res.* 98:417–440.
15. Rubinstein, J. T. 1988. Quasi-static analytical models for electrical stimulation of the auditory nervous system. Ph.D. thesis. University of Washington, Seattle, WA.
16. Rushton, W. A. H. 1927. The effect upon the threshold for nervous excitation of the length of nerve exposed, and the angle between current and nerve. *J. Physiol. (Lond.)*. 63:357–377.
17. Rushton, W. A. H. 1934. A physical analysis of the relation between threshold and interpolar length in the electric excitation of medullated nerve. *J. Physiol. (Lond.)*. 82:332–352.
18. Sachs, M. B., E. D. Young, and M. I. Miller. 1983. Speech encoding in the auditory nerve: implications for cochlear implants. *Ann. N.Y. Acad. Sci.* 405:94–113.
19. Scott, A. C. 1977. Neurophysics. John Wiley & Sons, New York.
20. Sten-Knudsen, O. 1960. Is muscle contraction initiated by internal current flow? *J. Physiol.(Lond.)*. 151:363–384.
21. Taylor, R. E. 1963. Cable theory. *Phys. Tech. Biol. Res.* 6:219–262.
22. Tranchina, D., and C. Nicholson. 1986. A model for the polarization of neurons by extrinsically applied electric fields. *Biophys. J.* 50:1139–1156.
23. Townshend, B., and R. L. White. 1987. Reduction of electrical interaction in auditory prostheses. *IEEE Trans. Biomed. Eng.* 34:891–897.